Effect of crosslink density on Sealant Properties Based on Silane- Modified Polyurethane

Mohammad Hassan Mahdavi Basir

m.mahdavi@ippi.ac.ir

Iran Polymer and Petrochemical Institute

Ali Salimi

Iran Polymer and Petrochemical Institute

Hossein Boohendi

Iran Polymer and Petrochemical Institute

Mohammad Zohuriaan-Mehr

Iran Polymer and Petrochemical Institute

Research Article

Keywords: Polyurethane, Sealant, Amino silane, Crosslink density, Mechanical properties

Posted Date: April 29th, 2024

DOI: https://doi.org/10.21203/rs.3.rs-4318287/v1

Additional Declarations: No competing interests reported.

Abstract

This study investigates the profound influence of crosslink density, stemming from both primary and secondary aminosilanes, on the properties of one-part polyurethane sealants. Through systematic experimentation, we elucidate the consequential effects of varying crosslinking agents on mechanical, thermal, and adhesive characteristics. Our results highlight the distinct impact of primary and secondary aminosilanes on the resulting material, offering valuable insights into tailoring specific properties for diverse applications. The chemical and physical structures of the one-part polyurethane sealants were investigated by nuclear magnetic resonance spectroscopy (NMR), Fourier transform infrared spectroscopy (FT-IR) and the mechanical properties were evaluated by tensile tests. The results reveal that silane-terminated moisture-curable polyurethanes can be successfully synthesized and cured with Dibutyltin Dilaurate catalysts. The comparative analysis underscores the nuanced interplay between crosslink density and material performance, paving the way for optimized formulations. This research enhances the fundamental understanding of crosslinking mechanisms, guiding the formulation of materials suitable for a wide array of applications.

1. Introduction

The synthesis of one-part amino silane-modified polyurethane, with the incorporation of either primary or secondary amino silanes, represents a significant leap forward in polymer chemistry. Also, offering a versatile and efficient method for tailoring material properties across a spectrum of applications [1]. Polyurethanes have long been valued for their exceptional mechanical properties, chemical resistance, and versatility, finding applications in adhesives, sealants, coatings, and elastomers [2–4].

This innovative process introduces a unique dual-functional enhancement mechanism that profoundly influences crosslink density and, consequently, material performance [5]. The integration of amino silanes into polyurethane formulations opens up new possibilities for improving and customizing these materials [2]. The amino silane compounds utilized in this synthesis feature both amino (NH2) functional groups and silane moieties, creating a dynamic system capable of simultaneous reactions with polyol and isocyanate components [2, 6].

The reactivity of primary and secondary amino silanes differs significantly, influencing the kinetics of the curing process [7, 8]. Primary amino silanes exhibit higher reactivity towards isocyanates compared to their secondary counterparts [2, 6]. This heightened reactivity arises from the increased nucleophilicity of primary amines, enabling them to readily engage with electrophilic isocyanate groups [2, 7]. Consequently, primary amino silanes play a leading role in the initial stages of the curing process, promoting the rapid formation of urethane linkages [2, 6]. In contrast, secondary amino silanes contribute to crosslinking density through subsequent reactions [9, 10]. While less reactive towards isocyanates, secondary amino groups come into play during the silanol-terminated reactions [2, 7]. These reactions involve the interaction of silanol groups, formed through the hydrolysis of the silane compounds, with the remaining hydroxyl groups on the polyol [11–13]. This dual reactivity of amino

silanes introduces a nuanced balance in the curing process, influencing the overall crosslinking density and, consequently, the material properties [14, 15].

The impact of crosslink density on material properties is fundamental. In polyurethane chemistry, crosslinking enhances mechanical strength, thermal stability, and resistance to environmental factors [16]. The dual-functional nature of amino silanes, participating in both urethane and siloxane linkages, establishes a robust network of crosslinks within the polymer matrix [17]. This intricate network not only reinforces the structural integrity of the cured polyurethane but also imparts resilience and durability [18].

Furthermore, the tailored integration of either primary or secondary amino silanes offers a unique avenue for fine-tuning the properties of the final material [19]. The varying reactivities of primary and secondary amino groups allow for precise control over the extent of crosslinking and the distribution of functional groups within the polymer matrix [14]. This level of control is particularly advantageous in applications where specific material properties, such as adhesion or flexibility, are critical.

The modification of polyurethane with amino silanes also leads to improvements in adhesion properties [20, 21]. The siloxane bridges formed by secondary amino silanes contribute significantly to enhanced adhesion by establishing strong bonds with diverse substrates. This feature is of immense significance in applications such as adhesives and coatings, where the ability to adhere to different surfaces is a critical performance criterion [22]. Importantly, this one-part adhesive system offers unique curing capabilities. The presence of water in moisture [23, 24], oxidation [25–27], and self-catalysis [28–30] serves as a trigger for the curing process. This moisture-curing ability makes the adhesive well-suited for applications where traditional heat curing may not be feasible [31]. The oxidation and self-catalysis mechanisms further broaden the range of environmental conditions under which the adhesive can effectively cure, adding versatility to its application in various settings [31].

Having explored the synthesis, reactivity aspects, and curing capabilities, the next crucial step involves a comprehensive characterization of the structures resulting from the incorporation of primary or secondary amino silanes. Advanced analytical techniques such as Fourier-transform infrared spectroscopy (FTIR) and nuclear magnetic resonance (NMR) provide insights into the molecular architecture and functional groups of the modified polyurethane [19].

The comparative analysis of properties between polyurethane modified with primary and secondary amino silanes adds another layer of understanding [11]. Mechanical testing, thermal analysis, and chemical resistance evaluations offer quantitative data on the impact of these amino silanes on the final material [11]. This comparative study aims to elucidate the nuanced differences in properties, aiding researchers and industries in selecting the most suitable modification for their specific applications.

In this article, our focus revolves around the synthesis of one-part amino silane-modified polyurethane, with a particular emphasis on investigating the impact of varying amino silane types on crosslink density and subsequent alterations in mechanical, thermal, and adhesion properties. The endeavor involves a

meticulous exploration of the distinct reactivity brought about by the primary and secondary amino silanes into the polyurethane matrix. By scrutinizing the ensuing changes in crosslink density, we aim to unravel the intricate effect of amino silane types on the resultant material characteristics. This study not only sheds light on the nuanced nuances of the synthesis process but also offers valuable insights into tailoring polyurethane materials for specific applications through the deliberate selection of amino silane types.

2. Experimental

2.1 Materials

Linear polypropylene glycol (PPG) with Mw of 2000 g. mol^{-1} was purchased from Isfahan Copolymer Company. Isophorone diisocyanate (IPDI) with isocyanate percentage of 35%, 3-aminopropyltrimethoxysilane (as primary amino silane) and bis (3-aminopropyltrimethoxysilane) (as secondary type amino silane) were obtained from Sigma Aldrich. The methyltriethylsilane (as a reactive diluent), dibutyltin dilaurate (as a substitution reaction catalyst), pyridine, toluene and isopropyl alcohol (as solvents), phenolphthalein and bromophenol blue (as indicators) and phthalic anhydride were all obtained from Merck.

2.2 Methods

2.3 Synthesis of urethane prepolymer (P-PU)

PPG (0.02 mol, 40 g) and dibutyltin dilaurate catalyst (0.02 g) were added gradually in a 100 ml four-neck glass reactor containing IPDI (0.05 mol, 11.12 g) at 75°C. Figure 1 shows this reaction pathway. The reaction continued under a mechanical stirrer at 250 rpm for 4 hours until the free isocyanate content remained constant. The percentage of free NCO of the prepolymer was calculated (ASTM D-2572) to obtain the required stoichiometric ratio in the next step.

2.4 Silane modification of P-PU

Methyltriethoxysilane as a reactive diluent was used to dilute 3-aminopropyltrimethoxysilane. The mixture of 3-aminopropyltrimethoxysilane (0.02 mol, ~ 3.59 g) and methyltriethoxysilane (0.01 mol, ~ 1.36 g) was gradually added to the prepared urethane prepolymer (0.01 mol, ~ 24.45 g) in a four-neck glass reactor equipped with a stirrer, condenser, and dry nitrogen purge. The reaction was continued at 50°C for 24 hours. The final product of this reaction was called ASPU1. Figure 2 shows the reactions between urethane prepolymer and amino silanes.

Note that sample ASPU2 was prepared in a similar synthesis route as that of Sample ASPU1 replacing 3-aminopropyltrimethoxysilane with bis (3-aminopropyltrimethoxysilane). Bis (3-aminopropyltrimethoxysilane) is a secondary type of amino silane with lesser reactivity than 3-

aminopropyltrimethoxysilane. Urethane prepolymer modification with bis (3-aminopropyltrimethoxysilane is shown in Fig. 2.

2.5 Determination of free NCO

To determine the unreacted isocyanate and/or isocyanate end groups in urethane prepolymer, the titration method was used according to ASTM D-2572 standard test method. This method may be well practiced in evaluation of the reaction progress of urethane prepolymer, as well as the silane modification of urethane prepolymer.

2.6 Spectroscopic characterization

The chemical structure of the prepared samples was studied using FTIR spectroscopy. The spectra were obtained in an EQUINOX 55 spectrometer (Bruker, Germany) in the range of 400–4000 cm^{-1} at a resolution of 4 cm^{-1}. The liquid sample was spread on a KBr tablet and dried at ambient temperature to form a uniform film of about 50-micrometer thickness.

^{1}H-NMR Spectroscopy was used to check and determine the chemical structure of the prepared samples. After dissolving in deuterated chloroform, the sample was analyzed using a ^{1}H-NMR device (Avance Dpx-400MHz, Bruker, Germany).

2.7 Cure study

Tack-free time is a measure of the surface cure time during the application of a substance, such as a coating or sealant. It is the point at which the substance has adhered to the surface and can provide maximum protection without being damaged or disrupted. The tack free time was used to measure the drying time of the samples according to EN-2-14187 standard test method. The test was carried out at 23 ± 2°C and a relative humidity of 90 ± 2%. Note that the relative humidity of 90 ± 2% was supplied through an aqueous solution of potassium nitrate in water.

The hardness (Shore A) of the cured sample was measured according to ASTM D-2240 standard test method with a hardness tester (TQC LD0550, Germany). At least five replicates on different points of the sample surface were conducted resulting in an average value and standard deviation. The hardness of the sample may be regarded as a good estimate of the degree of cure and or setting time which is an important factor in its curing process. For this purpose, the hardness of the resin was analyzed in different times from 1.5 to 150 hours (non-uniformly distributed, shorter time intervals at the beginning) at 23 ± 2°C and a relative humidity of ?50 ± 5%. The relative humidity of 50 ± 2% was supplied through 85wt% aqueous solution of potassium nitrate in water.

2.8 Thermogravimetry analysis (TGA)

The thermal stability of the cured samples was investigated using the TGA test (METTLER TOLEDO model, Switzerland). The test was carried out in nitrogen atmosphere, from 25 ºC to 600 ºC at a heating rate of 10 ºC. min^{-1}. The thermogravimetry data were also drawn as a derivative diagram and T_{onset},

$T_{20\%}$, $T_{50\%}$ and char yields at 600°C were reported. T_{onset} is the temperature at which the mass of the sample starts to deviate from the baseline. $T_{20\%}$ or $T_{50\%}$ are parameters that indicate the temperature at which 20% or 50% of the sample mass has been lost due to thermal degradation. char yield is a parameter that indicates the amount of residue left after the thermal degradation of a sample. It is expressed as a percentage of the initial sample mass and represents the fraction of the sample that has been converted into solid carbon or ash.

2.9 Dynamic mechanical thermal analysis (DMTA)

To check the dynamic mechanical thermal analysis (DMTA-TRITON model LG101, England), the samples were prepared in 40×10×2 mm dimensions. All the specimens were tested in a sinusoidal bending mode at a frequency of 1 Hz and heating rate of 5°C.min^{-1} from − 150 ºC to 100 ºC.

The crosslinking density; CLD can be quantitatively measured using Eq. 1.

$$E' = \frac{\rho RT}{M_C} \quad \text{Eq. 1}$$

where E' is the storage modulus of the rubbery plateau, $\boldsymbol{\rho}$ is the density of the amorphous polymer (1.08 g. cm^{-3}), R is the global gas constant, T is the absolute temperature at which rubbery state begins and M_c is the molecular weight between the crosslinking points.

2.10 Mechanical properties

The tensile test was performed according to ASTM D 412 standard test method. The main tensile properties such as the tensile strength, elongation at break, elastic modulus and area under stress-strain curve (toughness) of the prepared samples are obtained. The dumbbell-shaped samples were molded and cured in silicone molds. All the specimens were tested in an STM-20 model tensile machine (Santam, Iran) at a crosshead speed of 5 mm. min^{-1}. The tensile test of each sample was repeated five times resulting in an average value with a standard deviation.

2.11 Adhesion lap shear test

Single lap shear joints were fabricated and tested according to the ASTM-D1002 standard test method. The individual lap shear joints were prepared using aluminum 2024-T3 type and poly (methyl methacrylate); plexiglass sheets with dimensions of 100×25×1.5 mm^3. The substrates were first degreased with ethanol and acetone followed by roughening with 400 mesh sandpaper. Aluminum substrates were further chemically modified using 3 wt.% sodium dichromate solution in sulfuric acid (15 wt.%) according to ASTM D2093 standard test method.

In order to measure lap shear strength of modified urethane prepolymer, after the preparation of the substrates and their visual inspection, a thin layer of sealant with dimensions of 25x12.5x0.1mm was applied at the ends of the two substrates, which had an angle of 180 degrees. The samples were completely cured. The samples were stretched at a speed of 1.3 mm/min using (STM-20 model, Santam,

Iran). The test was repeated five times for each sample resulting in an average value and standard deviation

3. Results and discussions

The process typically starts with the hydrolysis of the silane compound, where it reacts with water to produce silanol groups. These silanol groups then undergo condensation reactions, forming siloxane linkages that bridge between polymer chains. Figure 3 shows curing mechanism of silane functional groups. This crosslinking imparts enhanced mechanical, thermal, and chemical properties to the cured material. Silane curing is widely employed in the production of adhesives, sealants, and coatings, offering improved durability and adhesion.

3.1 Spectroscopic characterization

The structure of PPG and IPDI as well as P-PU, ASPU1, and ASPU2 samples using FTIR and the structure of ASPU1, and ASPU2 samples using ^{1}H-NMR was investigated. The FTIR spectra of PPG and IPDI as well as P-PU, ASPU1, and ASPU2 samples are shown in Fig. 3.

Comparing FTIR spectra of PPG, IPDI, and P-PU in Fig. 4 shows the changes in functional groups during the synthesis of urethane prepolymer. The disappearance of the peak related to the functional group O-H, the appearance of a peak at the 1720 cm^{-1} (related to the C = O stretching vibration of the urethane group, red band) confirms the formation of urethane prepolymer with isocyanate end groups. The peak 2225 cm^{-1} (Fig. 4-c, green band), which is the result of the vibration of the NCO functional group, indicates the formation of a prepolymer with isocyanate end groups [32]. The remaining isocyanate functional group is eligible for the reaction with the amine functional group of amino silane compounds. The amount of remaining NCO (3.09%) confirms the data on the FTIR spectrum of the P-PU sample.

The carbonyl urethane group (NH-CO-O) shows a strong peak at 1717 cm^{-1} in Fig. 4a-e. The peak appearing at 1562 cm^{-1} in Fig. 4c-e corresponds to the stretching vibration of the N-H group [33]. The corresponding peak of the ether bonds (C-O-C) in PPG appears in the region of 1100 cm^{-1}. The corresponding peak of (S_i-O-C) group appears in the region of 817 cm^{-1}. The appearance of the peak is related to the urea carbonyl group (NH-CO-NH) at 1636 cm^{-1} in Fig. 4c-e is due to the reaction of the amino group in amino silanes with the NCO group in urethane prepolymer. The complete removal of the isocyanate peak in 2255 cm^{-1} is an indication of the reaction completion of the isocyanate group with the amine groups and hence, the complete conversion of urethane prepolymer to urethane prepolymer with trimethoxysilane end groups.

The ^{1}H-NMR spectra of samples ASPU1 and ASPU2 are shown in Fig. 5.

According to Fig. 5, the hydrogens adjacent to the etheric oxygen in the chain backbone are at 3.5 ppm, the CH_3 pendant group's hydrogens of the etheric chain are at 1.2 ppm, the CH_3 group corresponding to

the IPDI monomer is in the below 1 ppm and other methylene groups inside the IPDI ring appeared about 1.7 ppm. The peaks observed at about 5 ppm are related to amino/amide group hydrogens. In addition, peaks related to trimethoxysilane groups appeared at 3.5 ppm and hydrogens related to the carbon attached to the nitrogen atom appeared at 3.2 ppm.

3.2 Cure time

Surface drying time (Tack-free time) and hardness (Shore A) were used to check the curing time of the samples.

The surface dry time of the samples obtained by the Tack free time test is listed in Table 1.

Table 1
The data of tack-free times at 23°C and a relative humidity of 90 ± 2%

Sample	Time (h)
ASPU1	3:30
ASPU2	1:00

The surface dry time of the ASPU1 sample at 90% relative humidity is significantly longer than the surface dry time of the ASPU2 sample. The shorter dry time in sample ASPU2 may be attributed to the presence of more alkoxysilane functional end groups in ASPU2 than ASPU1 sample. The more alkoxysilane functional end groups, the much shorter curing time and or the more crosslink density.

the curing is a time-consuming process and the sample becomes harder as the number of crosslinking points increases. The more crosslinking points and/or the smaller the molecular mass between crosslinks (Mc), the harder the sample. This upward trend continues until reaching full curing after which the hardness of samples become plateau. Figure 5 shows the variations of sample hardness during curing time at 90% RH.

It is clear from Fig. 5 that the hardness increases sharply in the beginning and then flatten after over 100 hours. However, the sample ASPU1 experiences lower hardness values than those of sample ASPU2 at all respective curing times. The hardness of sample ASPU2 reached 85 (shore A) after over 100 hours higher than sample ASPU1 with 75 (shore A). The higher hardness value in sample ASPU2 may be well attributed to the ability of the secondary type silane to form more crosslink points [10]. Note that the start time of the hardness test for the ASPU1 sample was delayed more than for the ASPU2 sample, which was proportional to the drying time of the samples (tack-free time).

3.3 Thermogravimetry and DMTA properties

Figure 6 shows the thermogravimetric analysis (TGA) and differential thermogravimetric (DTG) curves of modified polyurethane with primary and secondary type amino silanes (ASPU1 and ASPU2).

The TGA curve shows the weight loss of the sample as a function of temperature. The DTG curve shows the rate of weight loss as a function of temperature. As it can be seen in Fig. 6, the TGA curve of ASPU1 showed three stages of weight loss. The first stage was due to the loss of moisture, the second stage was due to the decomposition of the less thermally stable polymer segments (Segments that do not have pendent silane groups), and the third stage was due to the decomposition of the more thermally stable polymer segments (Segments that have pendent silane groups). The TGA curve of ASPU2 showed two stages of weight loss. The first stage was due to the loss of moisture and the second stage was due to the decomposition of the polymer. In the ASPU2 sample, we have used bis (3-aminopropyltrimethoxysilane) for modification and this compound has more silane functional groups compared to 3-aminopropyltrimethoxysilane (2:1), it is more likely that all segments of the polymer have silane groups. It means all segments in ASPU2 are thermally stable to the same extent.

The DTG curves showed that the maximum rate of weight loss occurred at around 400°C for both ASPU1 and ASPU2. The initial temperature of destruction (T_{onset}) in both samples is almost the same and is at around 350°C. Both samples show almost the same degradation behavior up to the temperature of 400°C at which the weight loss is 20%; $T_{20\%}$. In comparison with sample ASPU2, a decrease of about 10°C in $T_{50\%}$ is observed for the sample ASPU1 with $T_{50\%}$ of 460°C. The char yield for ASPU1 and ASPU2 was 10% and 13%, respectively, at 600°C. The presence of silicon in the structure causes thermal stability, and because bis (3-aminopropyltrimethoxysilane) has twice the number of silane groups compared to 3-aminopropyltrimethoxysilane, therefore the thermal stability of ASPU2, which has a silane agent of the secondary type of bis (3-aminopropyltrimethoxysilane), is higher than the thermal stability of ASPU1, which has a silane agent of the primary type of 3-aminopropyltrimethoxysilane.[11]

Figure 7 shows loss factor curve (Tan δ) and storage modulus curves for the samples ASPU1 and ASPU2.

Note that the corresponding parameters extracted from DMTA were tabulated in Table 2.

Table 2
The corresponding parameters extracted from DMTA for ASPU1 and ASPU2 samples

Sample	Tan δ peak				rubbery region	
	T_g (°C)	Height	FWHM (°C)	Area (°C)	T/E' (°C/MPa)	Mc ($g.\ mol^{-1}$)
ASPU1	-32	0.42	29.41	17.74	27	241
ASPU2	-36	0.37	30.81	18.11	17	151

In the realm of one-part polyurethane-modified amino silane sealants, dynamic mechanical analysis reveals that ASPU1, characterized by a primary type amino silane, is less stiff than ASPU2 with a secondary type amino silane. As shown in Fig. 8, ASPU1 exhibiting a slightly lower storage modulus, its higher molecular weight between crosslinks (Mc) at 241 g/mol indicates a less tightly interconnected network, contributing to increased flexibility in ASPU1 compared to ASPU2. This difference in stiffness is further accentuated when considering the glass transition temperature (Tg). The Tg of ASPU1 at -32°C suggests a point at which the material transitions from a more flexible to a more rigid state. Contrastingly, ASPU2, featuring a slightly lower Tg of -36°C and the incorporation of a secondary amino silane, indicates a shift to a more rigid state at a lower temperature. While ASPU2 has a higher crosslink density, the Tg is influenced not only by crosslink density but also by molecular interactions and overall polymer structure. The presence of secondary amino silane in ASPU2 introduces specific molecular arrangements that impact the Tg differently than the primary amino silane in ASPU1. Molecular interactions and structural variations collectively contribute to the observed Tg differences, providing valuable insights into the intricate factors influencing the mechanical behavior of these sealants.

3.4 Mechanical properties

The tensile stress-strain curves of ASPU1 and ASPU2 are shown in Fig. 9. The corresponding parameters in tensile test were tabulated in Table 3.

Table 3
extracted data from Fig. 8

Sample code	Tensile strength (MPa)	Tensile modulus (MPa)	Toughness (J/m^2)	Elongation at break (%)
ASPU1	2.09 ± 0.53	8.16 ± 1.21	17.00 ± 3.06	38.06 ± 0.15
ASPU2	2.51 ± 0.48	8.77 ± 0.93	13.63 ± 3.46	32.90 ± 1.92

As it can be seen from Fig. 8, the tensile strength and modulus of the ASPU2 sample have increased compared to the ASPU1 sample similar to the modulus changes in DMTA. The use of a secondary type of amino silane agent in the ASPU2 sample creates more crosslinks with a higher density in the sample, so it resists the applied stress more than the ASPU1 sample. The elongation at break and the area under the stress-strain curve in the ASPU2 sample have decreased compared to the ASPU1 sample, and the ASPU2 sample has become more brittle, which can be attributed to the greater number of crosslinks in the ASPU2 sample because it reduces the chain freedom, elongation at break as well as the area under the stress-strain curve (toughness) [34].

Figure 10 The results of lap shear strength for the joints prepared from ASPU1 and ASPU2 on Aluminum and PMMA substrates

In examining the lap shear strength results, the consideration of cross-link density becomes particularly insightful. Despite ASPU2 exhibiting a higher cross-link density than Aspu1, the lap shear strength (shown in **Fig. 10**) of ASPU1 surpassed that of ASPU2 on both aluminum and PMMA sheet substrates. This intriguing observation prompts a deeper exploration of the interplay between various adhesive properties.

One notable factor contributing to this discrepancy is the inherent difference in surface energies of aluminum and PMMA. The aluminum substrate, with a surface energy of 0.868 N. m^{-1}, surpasses the significantly lower surface energy of PMMA at 0.041 N. m^{-1}. This substantial contrast in surface energies could play a pivotal role in dictating the adhesion behavior of the amino silane sealants. As ASPU1 demonstrates superior lap shear strength on both substrates, it suggests that its adhesive properties, such as compatibility with higher surface energy materials, may contribute to its enhanced bonding performance.

Moreover, while ASPU2 boasts a higher cross-link density, the effectiveness of an adhesive is not solely determined by this factor. Adhesion involves a complex interplay of chemical interactions, surface energies, and interfacial compatibility. The nuanced nature of these interactions may result in the observed performance trend, wherein the lap shear strength of ASPU2 lags behind despite its higher cross-link density. Future investigations should delve into the intricate dynamics of adhesive-substrate interactions to unravel the specific mechanisms influencing the bonding behavior of ASPU1 and ASPU2.

The failure mode was analyzed after the lap shear adhesion test. The respective fractured surfaces of the samples were captured by camera and are shown in Fig. 10.

Upon scrutinizing post lap shear test photographs (as shown in Fig. 11), distinctive failure modes emerged for ASPU1 and ASPU2, shedding light on their diverse adhesive behaviors. ASPU1 exhibited a cohesive failure, indicative of internal sealant cohesion being compromised. In contrast, the failure of ASPU2 demonstrated an adhesive nature, suggesting detachment at the sealant-substrate interface. Notably, ASPU2, characterized by a higher cross-link density as a secondary type amino silane modified polyurethane, showcased this adhesive failure. In ASPU1 sample, the internal forces in bulk are not strong enough to prevent the crack propagation through the adhesive layer. Whereas in ASPU2 sample, the higher crosslink density favors the adhesive modulus, hence result in crack propagation mostly not in adhesive layer but through interfacial region. That is why the adhesive mode is the dominant failure mode in sample ASPU2. As the modulus of the adhesive layer increases (as in ASPU2 sample), the possibility of crack growth through the interfacial region (adhesive failure mode) increases. The juxtaposition of cohesive failure in ASPU1 with the adhesive failure in ASPU2 underscores the intricate interplay between cross-link density, adhesive properties, and substrate interactions, offering crucial insights into the distinct behaviors of these amino silane sealants in lap shear applications.

4. Conclusion

In conclusion, our exploration of one-part amino silane-modified polyurethane has unveiled a versatile and efficient method for tailoring material properties. The strategic incorporation of primary and secondary amino silanes introduces a dual-functional enhancement mechanism, significantly influencing crosslink density and, consequently, material performance. The reactivity disparities between primary and secondary amino groups play a pivotal role in shaping the curing process kinetics. Primary amino silanes drive rapid urethane linkage formation, while secondary amino silanes contribute to crosslinking density through silanol-terminated reactions. This intricate balance offers precise control over crosslinking extent, enabling customization of material properties.

The impact of crosslink density on material properties is fundamental, enhancing mechanical strength and thermal stability. The dual-functional nature of amino silanes, participating in both urethane and siloxane linkages, establishes a robust network within the polymer matrix, reinforcing structural integrity and imparting resilience. The tailored integration of either primary or secondary amino silanes provides a unique avenue for fine-tuning material properties, addressing specific needs in applications where adhesion, flexibility, or other characteristics are critical.

Furthermore, the modified polyurethane demonstrates improved adhesion properties, particularly through the siloxane bridges formed by secondary amino silanes. The one-part adhesive system's moisture-curing ability makes it adaptable in environments where traditional heat curing is impractical. The oxidation and self-catalysis mechanisms further enhance its versatility across various settings. Our comprehensive characterization, utilizing advanced analytical techniques, offers insights into molecular structures and functional groups.

The comparative analysis between primary and secondary amino silane modifications, encompassing mechanical testing, thermal analysis, and adhesion evaluations, provides quantitative data on material performance. This research not only contributes to the understanding of synthesis nuances but also serves as a valuable resource for industries seeking tailored polyurethane materials for specific applications. Overall, the study emphasizes the nuanced impact of amino silane types on crosslink density and resultant material characteristics, paving the way for advancements in polymer chemistry and material science.

Declarations

Conflict of interests

There is no conflict to declare.

Author Contribution

All authors reviewed the manuscript

Acknowledgment

The authors thank the Iran Polymer and Petrochemical Institute (IPPI) for the financial support.

References

1. Subramani S et al (2007) Synthesis and properties of room temperature curable trimethoxysilane-terminated polyurethane and their dispersions. Polym Adv Technol 18(8):601–609
2. Xu J et al (2022) Recent advances in high-strength and high-toughness polyurethanes based on supramolecular interactions. Polym Chem 13(17):2420–2441
3. de Souza FM, Kahol PK, Gupta RK (2021) *Introduction to polyurethane chemistry*, in *Polyurethane Chemistry: Renewable Polyols and Isocyanates*. ACS Publications. pp. 1–24
4. Shabani M et al (2020) *Fixation of Carbon Dioxide Using Epoxy Resin: A Thermodynamics and Molecular Simulation Study*. in *Eco-friendly and Smart Polymer Systems 13*. Springer
5. Shi L et al (2023) In situ formed cross-linked polymer networks as dual-functional layers for high-stable lithium metal batteries. J Energy Chem 79:253–262
6. Aziz T et al (2021) Recent progress in silane coupling agent with its emerging applications. J Polym Environ, : p. 1–17
7. Hayichelaeh C et al (2018) Enhancing the silanization reaction of the silica-silane system by different amines in model and practical silica-filled natural rubber compounds. Polymers 10(6):584
8. Liu H, Harrod J (1992) Copper (I)-catalyzed cross-dehydrocoupling reactions of silanes and amines. Can J Chem 70(1):107–110
9. Peng H et al (2019) Understanding the effect of silane crosslinking reaction on the properties of PP/POE blends. Polym Bull 76:6413–6428
10. Du D et al (2020) Effects of different grafting density of amino silane coupling agents on thermomechanical properties of cross-linked epoxy resin. Polymers 12(8):1662
11. Karna N, Joshi GM, Mhaske S (2023) Structure-property relationship of silane-modified polyurethane: A review. Prog Org Coat 176:107377
12. Dodangeh F et al (2020) Synthesis and characterization of alkoxy silane modified polyurethane wood adhesive based on epoxidized soybean oil polyester polyol. Compos Part B: Eng 187:107857
13. Nomura Y et al (2007) Synthesis of novel moisture-curable polyurethanes end-capped with trialkoxysilane and their application to one-component adhesives. J Polym Sci Part A: Polym Chem 45(13):2689–2704
14. Zhao H et al (2017) Synthesis and investigation of well-defined silane terminated and segmented waterborne hybrid polyurethanes. New J Chem 41(17):9268–9275
15. Meng Y et al (2022) Synthesis and characterization of crosslinked castor oil-based polyurethane nanocomposites based on novel silane-modified isocyanate and their potential application in heat insulating coating. Polymers 14(9):1880

16. Trzebiatowska PJ et al (2018) The changes of crosslink density of polyurethanes synthesised with using recycled component. Chemical structure and mechanical properties investigations. Prog Org Coat 115:41–48
17. Dang G-p et al (2023) *Polyurethanes for Sealants*, in *Polyurethanes: Preparation, Properties, and Applications Volume 2: Advanced Applications*. ACS, pp 153–168
18. Moradi G et al (2020) Organoclay nanoparticles interaction in PU: PMMA IPN foams: Relationship between the cellular structure and damping-acoustical properties. Appl Acoust 164:107295
19. Gurunathan T, Chung JS (2016) Physicochemical properties of amino–silane-terminated vegetable oil-based waterborne polyurethane nanocomposites. ACS Sustain Chem Eng 4(9):4645–4653
20. Schreiber HP, Qin R, Sengupta A (1998) The effectiveness of silane adhesion promoters in the performance of polyurethane adhesives. J Adhes 68(1–2):31–44
21. Rodrigues VC et al (2023) Development and Study of a New Silane Based Polyurethane Hybrid Flexible Adhesive—Part 1: Mechanical Characterization. Materials 16(23):7299
22. Zhao Y et al (2022) A novel moisture-controlled siloxane-modified hyperbranched waterborne polyurethane for durable superhydrophobic coatings. Appl Surf Sci 587:152446
23. de Buyl F (2013) A generalized cure model for one-part room temperature vulcanizing sealants and adhesives. J Adhes Sci Technol 27(5–6):551–565
24. Pröbster M (2009) Versatile backbones for high-tech sealants and adhesives: Silane-Modified Polyether Sealants and Elastic Adhesives (Part 1), vol 6. ADHESION ADHESIVES&SEALANTS, pp 18–23
25. Brei MR et al (2017) Synthesis and thiol–ene photopolymerization of (meth) allyl-terminated polysulfides. J Appl Polym Sci 134(46):45523
26. Kurbangaleeva A, Kurkin A, Khakimullin YN (2012) Structure and properties of thiokol sealants modified with organosilanes. Russ J Appl Chem 85:432–436
27. Usmani A (1982) Chemistry and technology of polysulfide sealants. Polym-Plast Technol Eng 19(2):165–199
28. Graiver D, Farminer K, Narayan R (2014) *Soybean-Based Polyols and Silanols*, in *Soy-Based Chemicals and Materials*. ACS Publications. pp. 137–166
29. Gorelick L (1977) Bonding metal brackets with a self-polymerizing sealant-composite: a 12-month assessment. Am J Orthod 71(5):542–553
30. Yin Y et al (2008) Self-catalytic cross-linking reaction and reactive mechanism studies of α-aminomethyl triethoxysilanes for α, ω-dihydroxy poly (dimethylsiloxane). Eur Polymer J 44(7):2284–2294
31. Li X et al (2023) Preparation of siloxymethyl-modified silicone acrylate prepolymers with UV/moisture dual curability for applications in anti-smudge and anti-fingerprint coatings. Colloids Surf A 658:130669

32. Efstathiou K (2011) Synthesis and characterization of a Polyurethane Prepolymer for the development of a novel Acrylate-based polymer foam. Budapest University of Technology and Economics (BME), pp 1–57
33. Ihs A, Liedberg B (1989) Fourier transform infrared reflection-absorption spectroscopy of glycine absorbed upon copper. 7th Intl Conf on Fourier Transform Spectroscopy. SPIE
34. Hertzberg RW, Vinci RP, Hertzberg JL (2020) Deformation and fracture mechanics of engineering materials. Wiley

Figures

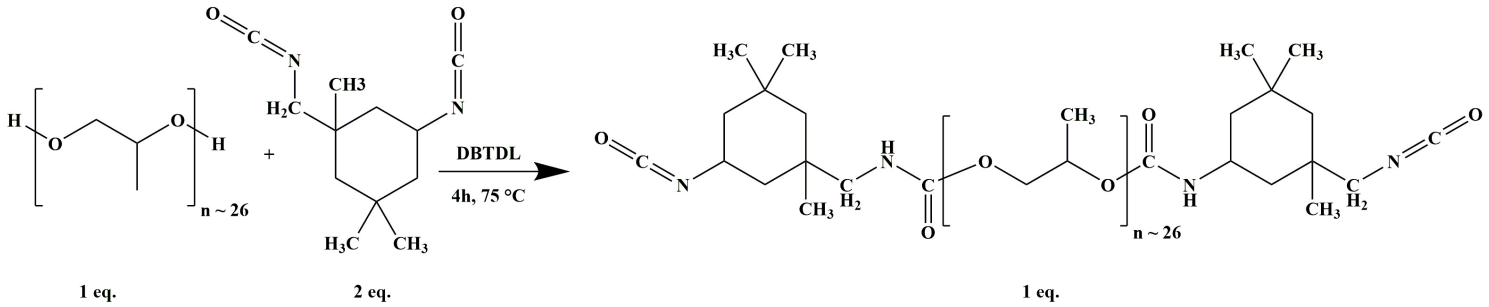

Figure 1

Schematic of urethane prepolymer synthesis

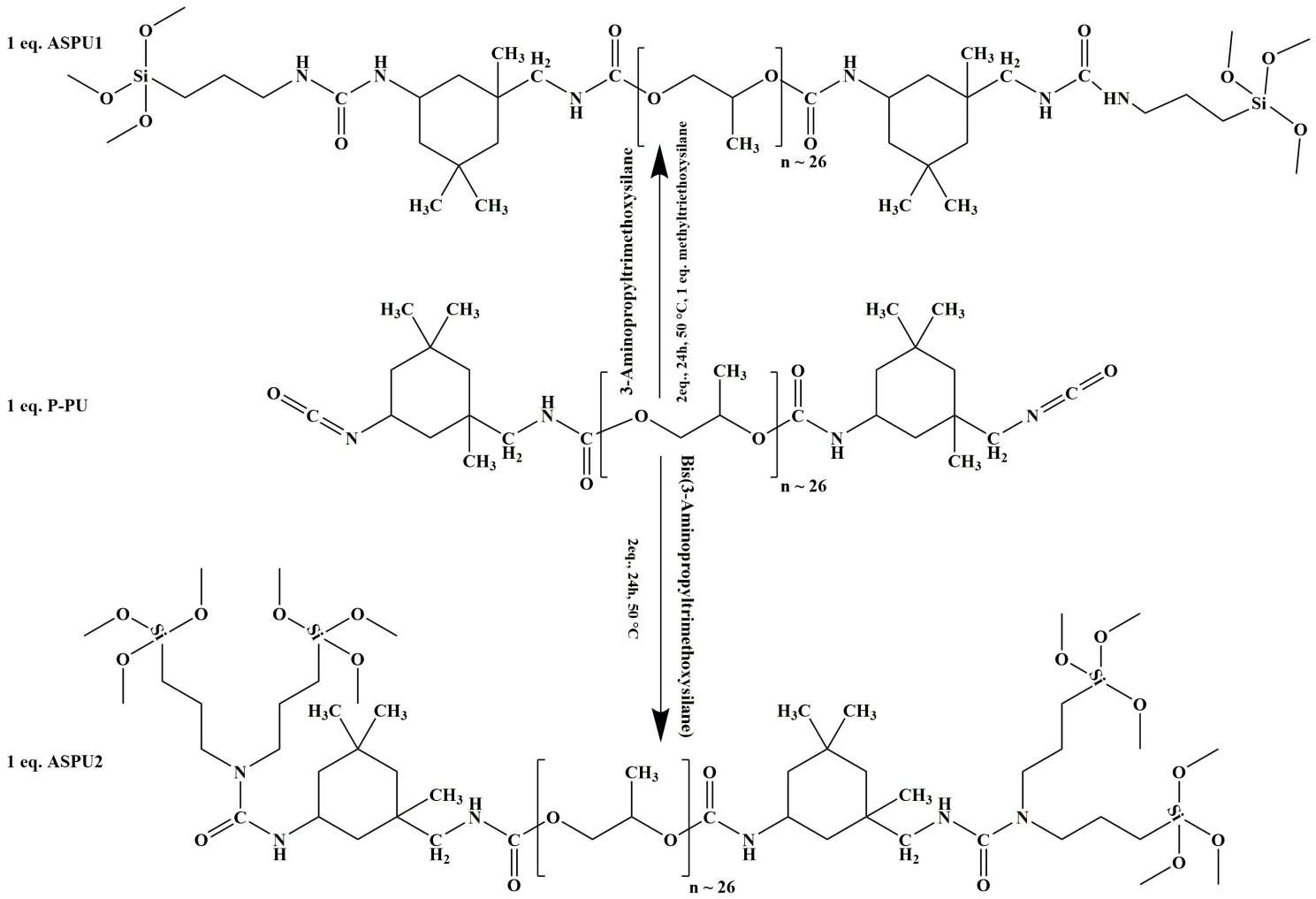

Figure 2

Schematic of urethane prepolymer modification with 3-aminopropyltrimethoxysilane and bis (3-aminopropyltrimethoxysilane

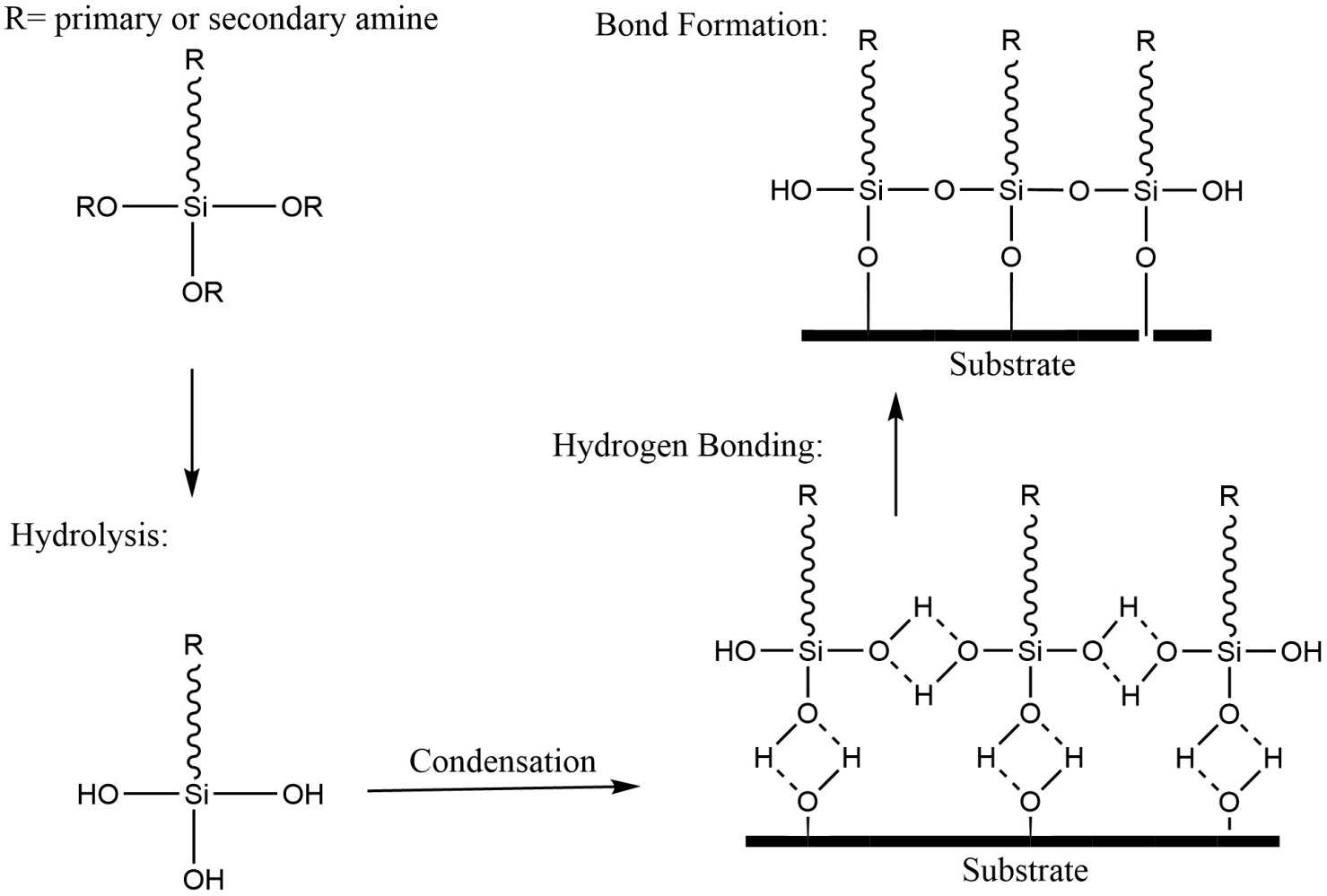

Figure 3

curing mechanism of silane functional groups.

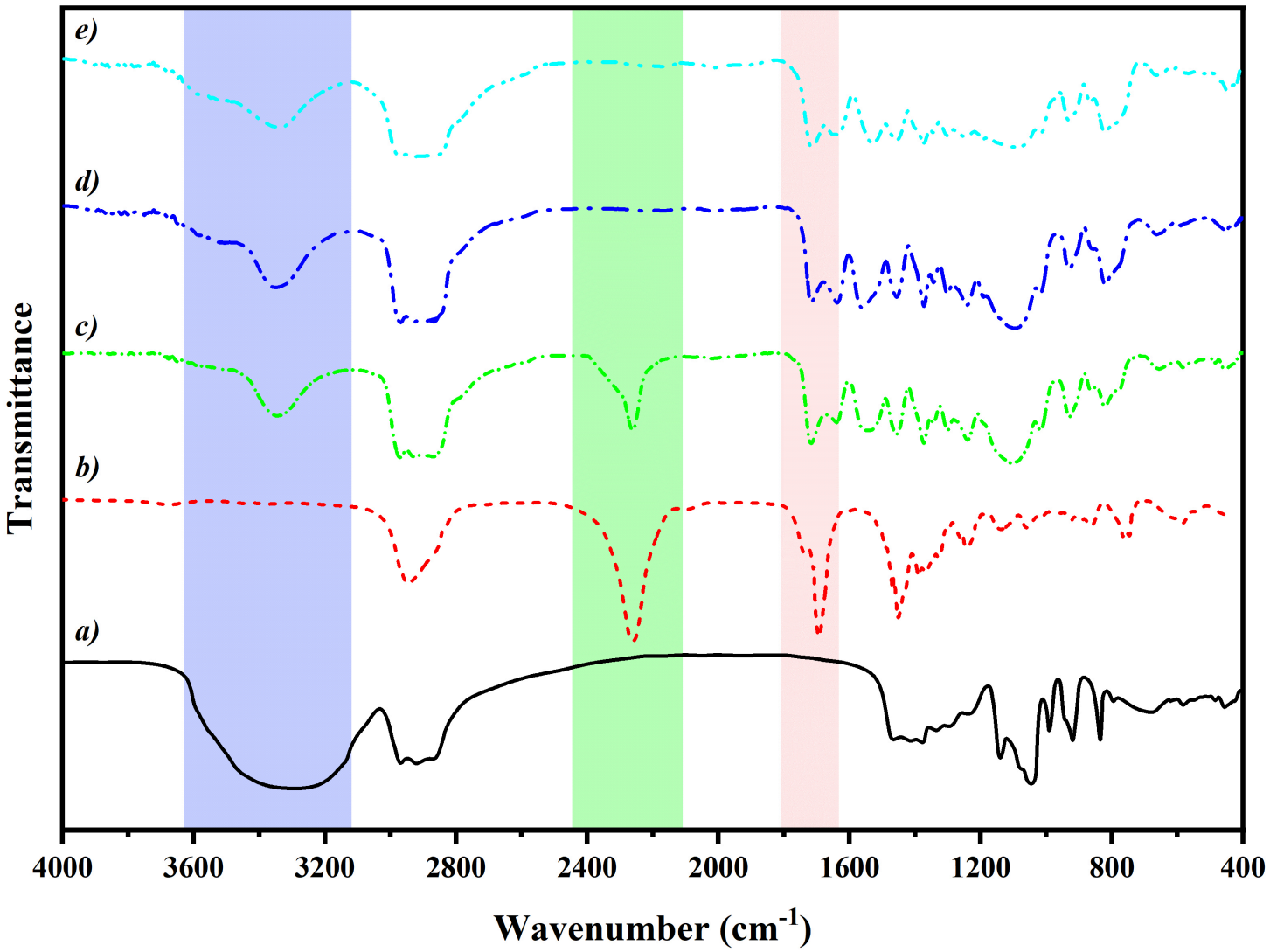

Figure 4

FTIR spectra of ***a***) PPG, ***b***) IPDI, ***c***) P-PU, ***d***) ASPU1 and ***e***) ASPU2; The red, green and blue bands show the wave numbers corresponding to the vibration of the carbonyl, isocyanate and hydroxyl groups, respectively, if they are present in the sample

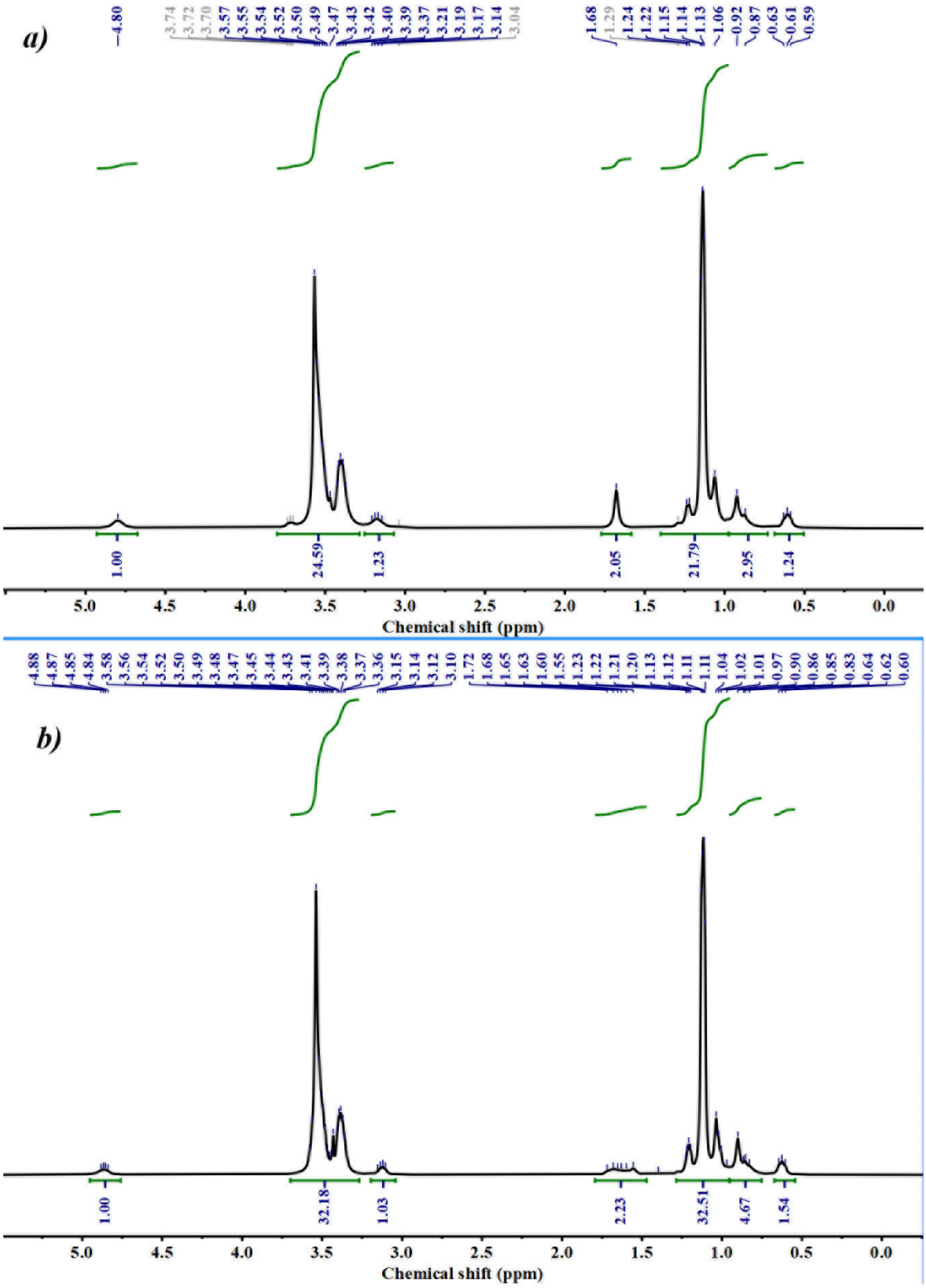

Figure 5

The H-NMR spectra of samples (a) ASPU1 and (b) ASPU2

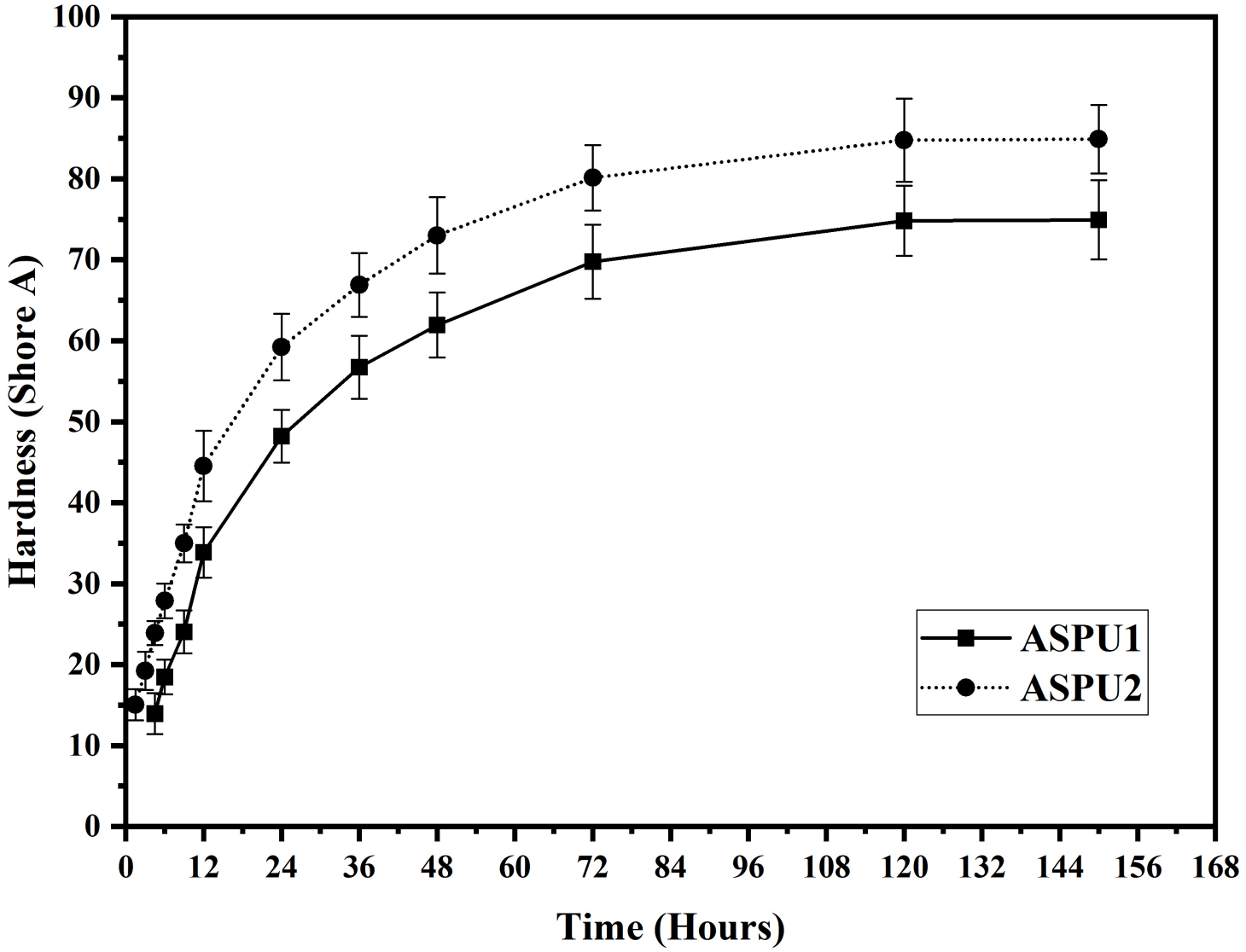

Figure 6

The variations of hardness of ***a***) ASPU1 and ***b***) ASPU2 samples

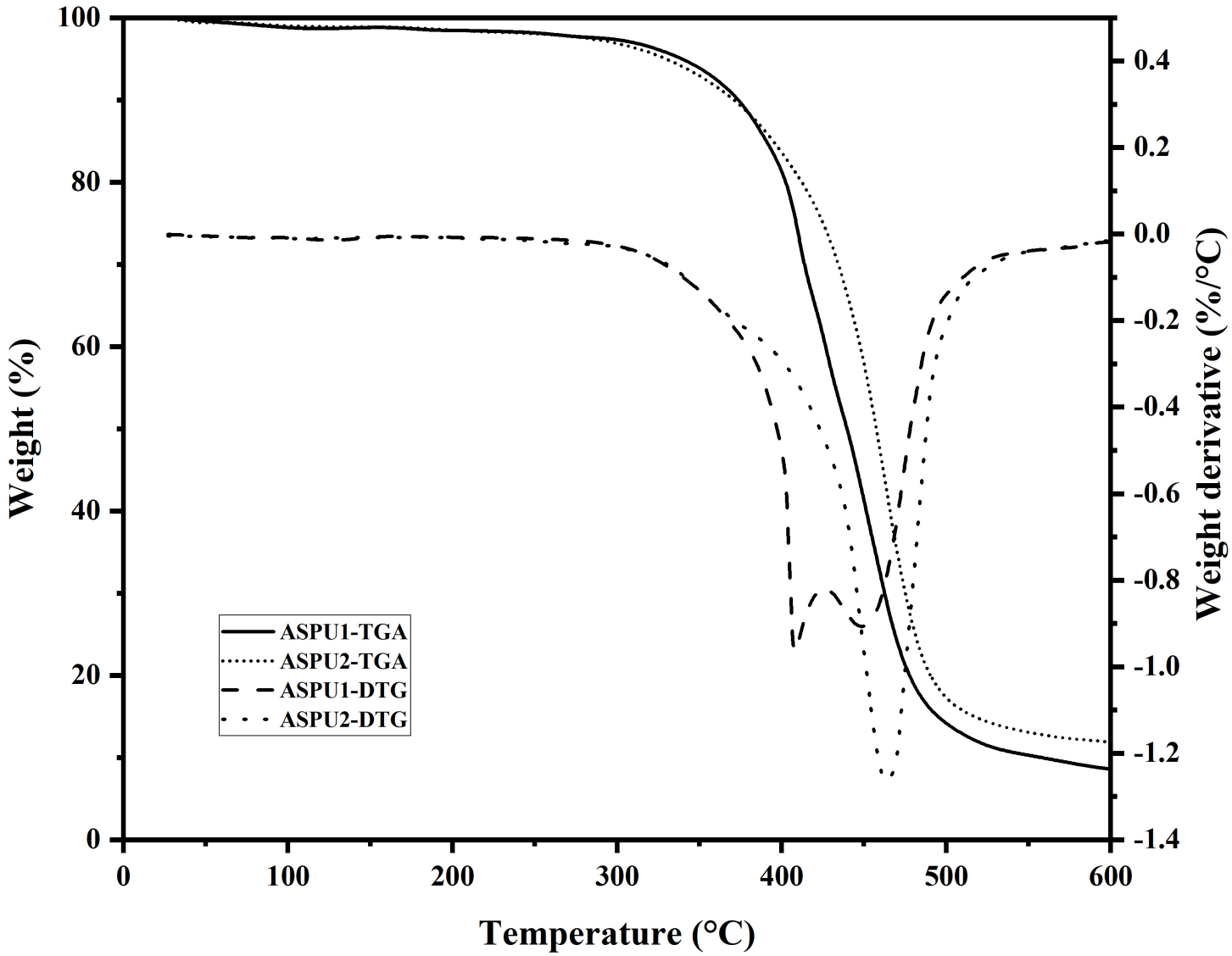

Figure 7

TGA and DTG curves of samples ASPU1 and ASPU2

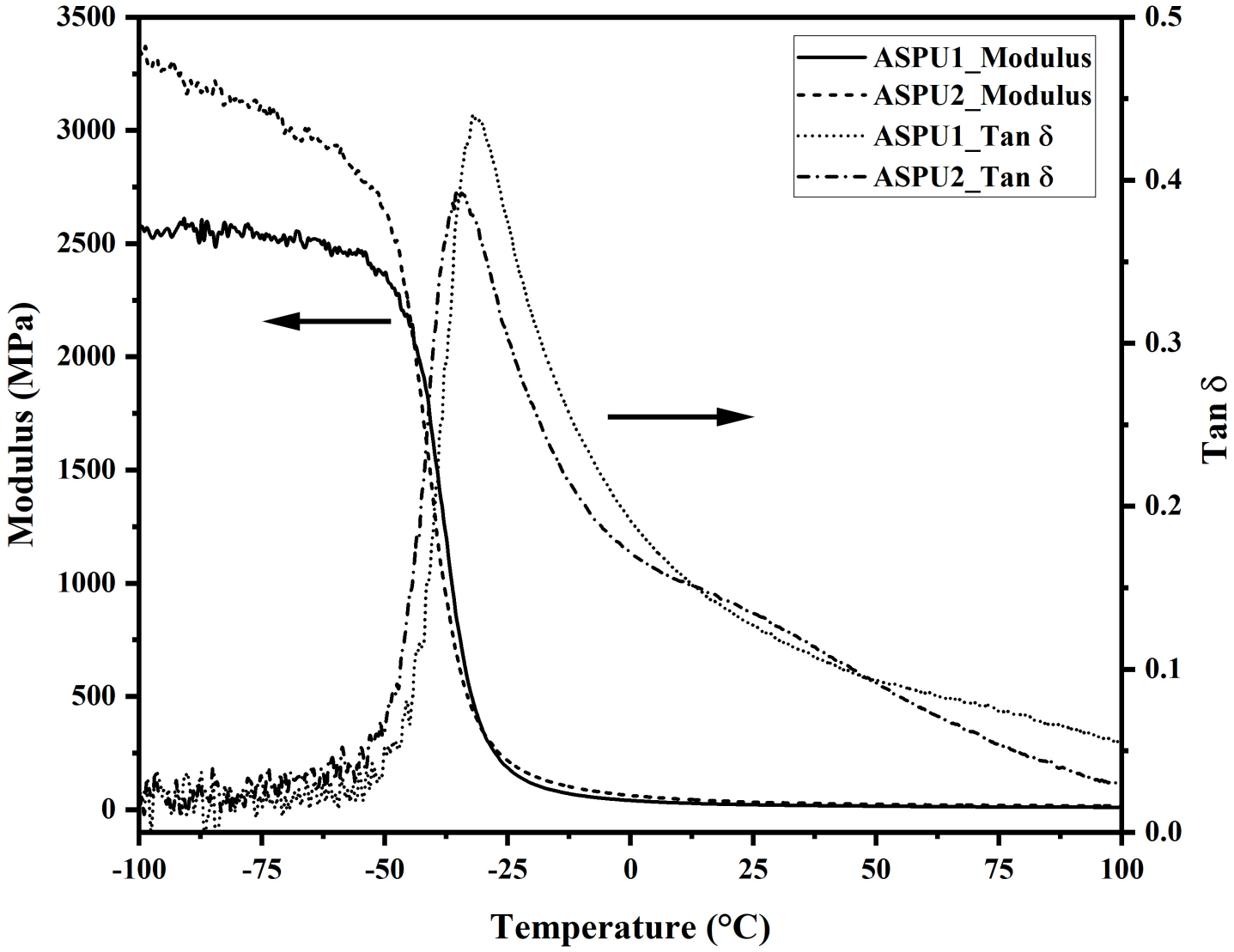

Figure 8

The storage modulus and tandcurves for ASPU1 and ASPU2 samples

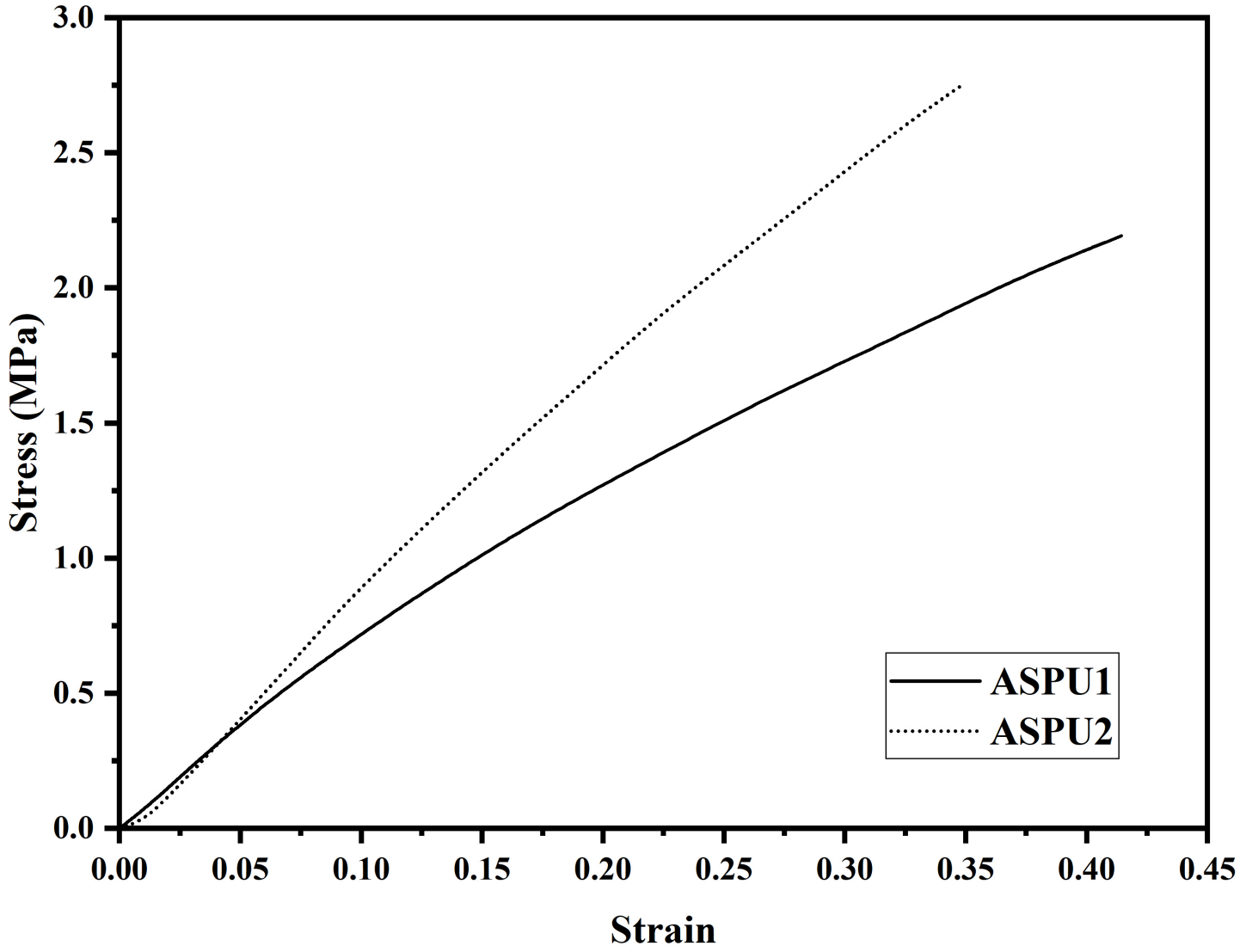

Figure 9

Tensile stress-strain curve of ***a***) ASPU1 and ***b***) ASPU2

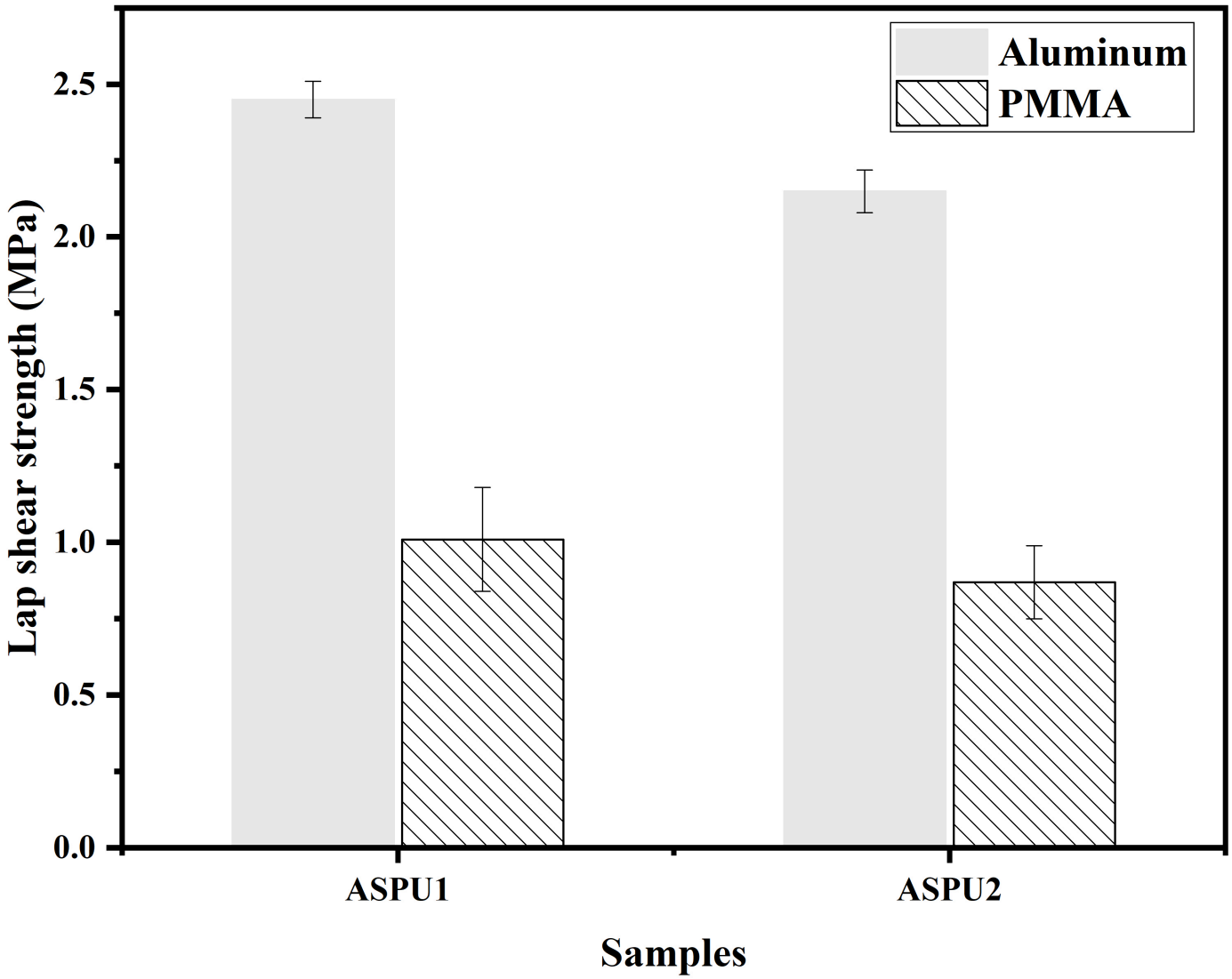

Figure 10

The results of lap shear strength for the joints prepared from ASPU1 and ASPU2 on Aluminum and PMMA substrates

Figure 11

Separation surface images of ASPU1 and ASPU2 samples on an aluminum substrate